Article

Innovative Analytical Methodology Combining Micro-X-Ray Diffraction, Scanning Electron Microscopy-Based Mineral Maps, and Diffuse Reflectance Infrared Fourier Transform Spectroscopy to Characterize Archeological Artifacts

Carolina Cardell, Isabel Guerra, Julia Romero-Pastor, Giuseppe Cultrone, and Alejandro Rodriguez-Navarro

Anal. Chem., **2009**, 81 (2), 604-611 • DOI: 10.1021/ac8022444 • Publication Date (Web): 19 December 2008

Anal. Chem. **2009,** *81,* 604–611

Innovative Analytical Methodology Combining Micro-X-Ray Diffraction, Scanning Electron Microscopy-Based Mineral Maps, and Diffuse Reflectance Infrared Fourier Transform Spectroscopy to Characterize Archeological Artifacts

Carolina Cardell,*,† Isabel Guerra,‡ Julia Romero-Pastor,† Giuseppe Cultrone,† and Alejandro Rodriguez-Navarro†

Department of Mineralogy and Petrology, Faculty of Science, and Scientific Instrumentation Centre, University of Granada, Campus Fuentenueva s/n, 18071 Granada, Spain

Excavations at the 14th century Moorish rampart (Granada, Spain) unearthed a brick oven alongside black ash and bone stratigraphic layers. In situ evidence suggests the oven served to fabricate a wall coating including powdered burnt bones. Original ad hoc analyses improved on conventional methods were used to confirm this hypothesis. These methods enable (i) nondestructive micro-X-ray diffraction (μ-XRD) for fast mineralogical data acquisition ($\sim$10 s) and moderately high spatial ($\sim$500 μm) resolution and (ii) identification and imaging of crystalline components in sample cross-sections via mineral maps, yielding outstanding visualization of grain distribution and morphology in composite samples based on scanning electron microscopy-energy dispersion X-ray spectrometry (SEM-EDX) elemental maps. Benefits are shown for applying diffuse reflectance infrared Fourier transform spectroscopy (DRIFTS) vs transmittance-FT-IR (T-FT-IR) to analyze organic and inorganic components in single samples. Complementary techniques to fully characterize artifacts were gas chromatography/mass spectroscopy (GC/MS), optical microscopy (OM), conventional powder XRD, and ^{14}C dating. Bone-hydroxyapatite was detected in the coating. Mineralogical transformations in the bricks indicate oven temperatures well above 1000 °C, supporting the hypothesis.

The synergy between archeology and scientific disciplines for better understanding archeological material is now indebatable.[1−5] The main goals in characterizing historic objects are preservation and investigation of the knowledge and technology used in their manufacture. Such information is essential to evaluate cultural and technological aspects of past societies and to further determine the temporal and geographical transfer of technology.[6−8] Archaeological objects comprise a wide variety of composite materials made up of complex mixtures of natural and artificial components (organic and inorganic). Additionally exposure of these artifacts to different environmental conditions (burial, refiring scenarios, pollution) may lead to new constituents and byproducts.[4,8,10] This makes artwork characterization a challenge. Difficulties multiply when sparse and microsize components have to be identified. Moreover, since bulk analyses do not inform regarding the distribution of these components, more detailed microanalyses are needed. A very powerful means of providing a concise overview of the object under study is the chemical information that can be visualized in the form of element maps;[9−13] however, mineral maps, applied somewhat in geology but not yet in heritage science, would be more useful.[14] Microtextural and structural characteristics of artifacts can provide key information regarding manufacturing techniques and thus for conservation purposes.[8,11,15]

* Corresponding author. Carolina Cardell, Department of Mineralogy and Petrology, Faculty of Science, University of Granada, Fuentenueva s/n, 18071 Granada, Spain. Phone: +34 958242725. Fax: +34 958243368. E-mail: cardell@ugr.es.

† Department of Mineralogy and Petrology, Faculty of Science.

‡ Scientific Instrumentation Centre.

(1) Damiani, D.; Gliozzo, E.; Memmi-Turbanti, I.; Spangenberg, J. E. *Archaeometry* **2003**, *45*, 341–354.

(2) Marengo, E.; Aceto, M.; Robotti, E.; Liparota, M. C.; Bobba, M.; Pantò, G. *Anal. Chim. Acta* **2005**, *537*, 359–375.

(3) Salvado, N.; Buti, S.; Tobin, M. J.; Pantos, E.; Prag, A.; Pradell, T. *Anal. Chem.* **2005**, *77*, 3444–3451.

(4) Cotte, M.; Susini, J.; Metrich, N.; Moscato, A.; Gratziu, C.; Bertagnini, A.; Pagano, M. *Anal. Chem.* **2006**, *78*, 7484–7492.

(5) Szczepaniak, M.; Nawrocka, D.; Mrozek-Wysocka, M. *Appl. Phys. A: Mater. Sci. Process.* **2008**, *90*, 89–95.

(6) Maravelaki-Kalaitzaki, P.; Kallithrakas-Kontos, N. *Anal. Chim. Acta* **2003**, *497*, 209–225.

(7) Martín-Gil, J.; Martín-Gil, F. J.; Ramos-Sánchez, M. C.; Martín-Ramos, P. *Environ. Sci. Pollut. Res.* **2005**, *12*, 285–289.

(8) Cardell, C.; Navarrete, C. *Stud. Conserv.* **2006**, *51*, 161–176.

(9) Cardell, C.; Yebra, A.; Van Grieken, R. *Microchim. Acta* **2002**, *140*, 9–14.

(10) Maravelaki-Kalaitzaki, P. *Anal. Chim. Acta* **2005**, *532*, 187–198.

(11) Vazquez-Calvo, C.; Alvarez de Buergo, M.; Fort, R.; Varas, M. J. *Mater. Charact.* **2007**, *58*, 1119–1132.

(12) Cotte, M.; Welcomme, E.; Sole, V. A.; Salome, M.; Menu, M.; Walter, P. H.; Susini, J. *Anal. Chem.* **2007**, *79*, 6988–6994.

(13) Lau, D.; Villis, C.; Furman, S.; Livett, M. *Anal. Chim. Acta* **2008**, *610*, 15–24.

(14) Smeink, R. G.; Leerdam Van, G. C.; Mahy, J. W. G. *Miner. Eng.* **2005**, *18*, 247–255.

(15) Cultrone, G.; Rodríguez-Navarro, C.; Sebastián, E.; Cazalla, O.; De la Torre, M. J. *Eur. J. Mineral.* **2001**, *13*, 621–634.

10.1021/ac8022444 CCC: $40.75
Published on Web 12/19/2008

Figure 1. A general view of the 14th century Moorish rampart in the Albayzín quarter of Granada. The circular holes have a 10 cm diameter.

Analysis of artwork is more restricted than other materials characterization fields due to severe limitations imposed on sampling. There is an increasing demand for nondestructive or microanalytical techniques that minimize as much as possible the amount of analyzed sample without compromising the quality of results and multiple component analysis in single microsamples is demanded. Fascinating results on artwork characterization are emerging from synchrotron radiation based-techniques.[4,16−18] The literature also reports the effectiveness of certain analytical techniques when used individually to typify artworks, such as Raman spectroscopy.[19,20] Unfortunately, however, these cutting-edge analytical instruments are often inaccessible for conservators and archeologists, being both uncommon (in laboratories) and costly. Consequently, alternative multiple analytical approaches, often designed ad hoc for characterizing specific artworks, are emerging to provide fully comprehensive material characterization.[10,21,22]

In this work we apply a novel combination of analytical techniques to study artifacts found during excavations in the Albayzín quarter of Granada (UNESCO World Cultural Heritage). The final goal is to accomplish restoration of the Moorish wall (Figure 1) built by the Nasrid ruler Yusuf I (1333−1354, who also built the Comares Palace at the Alhambra). Excavations discovered a brick oven and well-defined stratigraphic layers of black ash and bones. In situ examinations revealed evidence of melting processes in the bricks, indicating oven temperatures well above those required to fire Nasrid bricks and pottery (800−850 °C).[23] This, in addition to the presence of burnt bones, suggested the theory that the oven was used to fabricate a special wall coating, including powder burnt bones for that purpose.

The ancient decorative and protective layers that cover external surfaces of architectural heritage (patinas) have, over the last 2 decades, been the subject of multidisciplinary analyses in archeology, conservation, and chemistry.[7,10,24−26] Patinas have been a popular finishing for building exteriors and walls since ancient times mainly for aesthetic and protective reasons.[7] Setting aside their controversial origin (whether natural, biological, or artificial), their characterization is essential for purposes of conservation and knowledge of decoration techniques. The ancient mixture applied to create a patina could include lime and/or gypsum, water, natural pigments (e.g., iron oxides/hydroxides), organic additives (milk, blood, cheese, egg, urine, lard, oil, wax. . .), silicates (quartz, feldspar, and clay minerals), calcium oxalates, and calcium phosphates. This latter could be linked to the application of milk-derived, calcium caseinate-based protective treatments, the presence of egg white, algae,[24] and burnt bones.[7] Of particular interest is the occurrence of powdered burnt bone identified in Greco-Latin, Celtic, and Medieval Christian monuments,[7] but never, to our knowledge, in Medieval Moorish constructions. More importantly, unlike the present case, the literature reports neither archeological evidence of bones used as raw materials nor ovens to burn them.

In this paper, we present novel multianalytical routines for the characterization of the diverse archeological artifacts mentioned above. The "in house" protocols were designed ad hoc combining complementary nondestructive and microdestructive microscopic, molecular, and diffraction analytical techniques and adapting them specifically for each artifact studied. The benefits and limitations of each technique are put forward.

EXPERIMENTAL SECTION

Methodological Approach to Characterize Oven Bricks. *X-ray Diffraction (XRD) Methods.* Two XRD methods were used to identify the crystalline phases present in the bricks. Conventional powder XRD was applied to determine the bulk mineralogical composition as described elsewhere.[15] Brick samples (∼0.5 g) were milled in agate mortar to <40 μm particle size prior to analysis. The razor tamped surface method[27] was used to attain random particle orientation. Automatic acquisition, evaluation, and identification of minerals were carried out using XPowder software.[28] Quantitative analysis of mineral phases was done using the full data contained in the PDF2 database and nonlinear squared minimums on the full-profile fitting of the diffractograms. Phases weighting was calculated using the Normalized RIR Method.[29] An important advantage of this methodology is that it requires no internal standard.

To accurately explore the temperature-related mineral changes that occurred during the brick refiring process, we analyzed the mineralogical composition of bricks at different points using an X-ray single-crystal diffractometer equipped with an area detector (Smart Apex D8; Bruker, Germany). This type of diffractometer uses a small X-ray beam (typically 50−500 μm), allowing point analyses of a selected area in the sample of a few tens of

(16) Hermes, A. C.; Davies, R. J.; Greiff, S.; Kutzke, H.; Lahlil, S.; Wyeth, P.; Riekel, C. *Biomacromolecules* **2006**, *7*, 777–783.
(17) Correia, A. M.; Oliveira, M. J. V.; Clark, R. J. H.; Ribeiro, M. I.; Duarte, M. L. *Anal. Chem.* **2008**, *80*, 1482–1492.
(18) Genestar, C.; Pons, C. *J. Cult. Herit.* **2003**, *4*, 291–298.
(19) Perardi, A.; Appolonia, L.; Mirti, P. *Anal. Chim. Acta* **2003**, *480*, 317–325.
(20) Clark, R. J. H. *Appl. Phys. A: Mater. Sci. Process.* **2007**, *89*, 833–840.
(21) Pérez-Alonso, M.; Castro, K.; Álvarez, M.; Madariaga, J. M. *Anal. Chim. Acta* **2004**, *554*, 379–389.
(22) Castro, K.; Sarmiento, A.; Martínez-Arkarazo, I.; Madariaga, J. M.; Fernández, L. A. *Anal. Chem.* **2008**, *80*, 4103–4110.
(23) De la Torre-Lopez, M. J.; Rodríguez-Gordillo, J.; Sebastián, E. *Miner. Petrogr. Acta* **1992**, *26*, 171–179.
(24) Alvarez de Buergo, M.; Fort, R. *Constr. Build. Mater.* **2003**, *17*, 83–89.
(25) Lazzarini, L.; Salvadori, O. *Stud. Conserv.* **1989**, *34*, 20–26.
(26) Fassina, V. *Sci. Total Environ.* **1995**, *167*, 185–203.
(27) Zhang, G.; Germaine, J. T.; Martin, R. T.; Whittle, A. J. *Clays Clay Miner.* **2003**, *51*, 218–225.
(28) Martín-Ramos, J. D. Using XPowder: A software package for Powder X-ray diffraction analysis. www.xpowder.com, 2004 (GR 1001/04. ISBN 84-609-1497-6).
(29) Chung, F. H. *J. Appl. Crystallogr.* **1974**, *7*, 519–525.

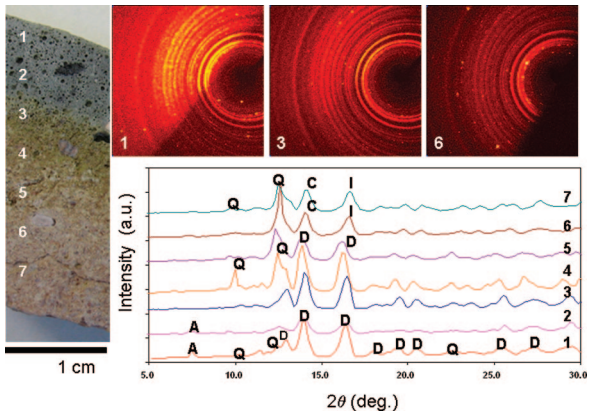

Figure 2. Mineral composition evolution along the brick cross-section determined by selected area X-ray diffraction. Brick macroscopic view displaying the color gradation due to refiring scenarios. Numbers indicate the different analyzed points (left). 2D diffraction patterns of selected points along the cross-sectioned brick (top). Two distinct types of Debye−Scherrer rings are displayed, some spotty and some continuous. Each ring type is associated with a different mineral. At the bottom are shown the calculated powder diffraction patterns from which the mineral phases present in the different points along the brick cross-section have been identified: A (anorthite), Q (quartz), D (diopside), C (calcite), I (illite).

micrometers in diameter. Thus, this instrument allows microanalyses of the mineralogical composition of the sample in situ and in a nondestructive mode. Among other benefits, it improves limit detections of minor mineral phases scattered within the sample. Diffraction data were analyzed with XRD2Dscan, a specially designed Windows application for polycrystalline materials characterization that analyzes two-dimensional (2D) diffraction patterns.[30] This software extracts information regarding sample mineralogical composition and microtextural characteristics of polycrystalline samples from the 2D diffraction patterns.

Experimental conditions used for μ-XRD analyses were Mo Kα radiation, 50 kV acceleration voltage, 30 mA filament current, 60 mm sample-to-detector distance, 500 μm collimator diameter, and 10−20 s exposure times. Measurements were done in the reflection mode at standard conditions with goniometer angular positions set at $2\theta = 20$, $\omega = 10$, $\phi = 90$, and $\chi = 54.749$ deg. Typical diffraction patterns consist of concentric rings, i.e., Debye−Scherrer rings like the one displayed in Figure 2, which results from the intersection of diffraction cones with the flat detector. The ring radius is related to the 2θ angle of a specific set of hkl planes satisfying the Bragg diffraction condition. The XRD2DScan software was used to calculate from the 2D pattern the equivalent powder diffractogram by radially integrating pixel intensities. From the calculated 2θ scan, the mineral phases present in the sample were identified using the XPowder software and the PDF2 database.[28] For μ-XRD analyses the brick sample was cut perpendicularly to the surface expose to the refiring-temperature (Figure 2). Samples of $\sim 25 \times 10 \times 10$ mm^3 requiring no preparation were adhered to a sample holder (3 mm diameter rod) and placed in the goniometer head of the diffractometer. To identify the mineral evolution upon refiring (mineralogical changes depend on temperature)[15] along the brick cross-section and establish the temperatures penetration depth in the brick, μ-XRD was employed every 3 mm over the brick profile (seven profile points).

Microscopic Techniques. A first petrographical examination of the brick to obtain an overview of its mineral composition, texture, and structure was done by means of optical microscopy (OM) using a polarized light microscope (Olympus BX60) equipped with digital microphotography unit (Olympus DP10). Then a detailed analysis of the microtexture and chemical composition, enabling one to distinguish the mineral reactions and changes suffered upon refiring, was performed with a scanning electron microscope SEM Leo 1430VP coupled with an EDX microanalysis (SEM-EDX) INCA 350 version 17 Oxford Instrument. Images were acquired in backscattered electron (BSE) and secondary electron (SE) modes. These modes are complementary, since SE provides information on the texture and structure while BSE identifies elemental composition. Single point elemental analyses and X-ray maps were acquired. The SEM-EDX working conditions were 500 pA filament current and 10 eV/ch resolution for pinpoint analyses, and 1 nA filament current and 20 eV/ch resolution for map acquisition. The beam energy used was 20 keV. Maps of 256 × 192 pixels were obtained in selected areas with 500 frames and dwell time of 10 ms. To study the samples under OM and SEM-EDX polished thin sections (~30 μm thick) were prepared (from resin-embedded samples) and carbon-coated to be further analyzed with SEM-EDX. A full explanation of the sample preparation can be found elsewhere.[11]

Methodological Approach to Characterize Wall Coating. *X-ray Diffraction Method.* Two nondestructive XRD methods were used to identify the crystalline phases present in three coating samples taken from different areas (where there was a certain assurance that the material was original). First, μ-XRD was applied directly to the surface coatings using experimental conditions similar to those specified for the oven bricks. A chip sample of $\sim 10 \times 10 \times 3$ mm^3 without preparation was placed onto an adhesive carbon tab (to minimize background interferences) and mounted on the goniometer head of the diffractometer, and single point analyses were done. This is not an entirely efficient method for identifying very fine and scarce crystal amounts of a specific mineral, since as mentioned, data measurements are spottily acquired. Thus, to detect the hydroxyapatite (HAp, $Ca_{10}[PO_4]_6[OH]_2$, the main bone component) mineral sought in the coating, a second XRD method using a Bruker D8 Powder Advance diffractometer was employed. To this end, the same sample was analyzed after placing it onto a zero background silicon plate with no preparation. Diffraction data were recorded using Cu Kα radiation, tube running at 40 kV, 40 mA, 0.02 deg step size, 20 s integration time, and 15 rpm rotation speed (spin mode). Diffraction patterns were scanned over a $15° < 2\theta < 70°$ range. The total data acquisition time was 15 h. This XRD method is time-consuming and thus more expensive than the μ-XRD routine but enables identification of minerals scarcely present in composite materials. In both XRD methods, minerals were identified using the XPowder software and the PDF2 database.[28]

Microscopic Techniques. Microscopic characterization of the coating was similar (sample preparation and analytical instrument) to that employed for the bricks. The petrographical characteristics,

(30) Rodríguez-Navarro, A. B. *J. Appl. Crystallogr.* **2006**, *39*, 905–909.

raw materials composition, and state of coating conservation were first examined by OM. Then SEM-EDX analyses were performed. Since one of the main goals of this work was the precise identification/visualization of HAp, mineral maps were compiled from elemental distribution maps by applying the Phasemap tool implemented in the Inca 350 version used in this work. This software identifies mineral phases using ternary element plots of specific pixel information from montaged X-ray maps. To this end, the operating SEM-EDX conditions were 500 pA filament current and 10 eV/ch resolution for single analyses and 1 nA filament current and 20 eV/ch resolution for element map acquisition. The beam energy used was 20 keV. Maps of 1024 × 768 pixels were obtained in selected areas with 500 frames and a dwell time of 10 ms by using the Smart maps software. For mineral maps performance, the INCA Phasemap software was employed by selecting three map images as source data for scatter plots and the pixel information over ternary diagrams. The procedure for mineral map acquisition involves the use of the so-called "ternary phase diagrams". The software generates mineral maps of the distribution of the relative concentration for up to three elements specified by the user with the collected matrix of EDX spectra. The element information embedded in each image pixel is rearranged in such a way that regions of similar (ternary) composition can be determined in the phase diagram. Superposition of images obtained from different "ternary phase diagrams", represented as a false color map, then yields a "phase map". To give a realistic reconstruction of mineral distribution in the cross-sectioned sample, the obtained mineral map must be overlapped onto the BSE image. The quantitative approach was done with the "Point & ID" tool implemented in the software. Improved quantitative results were obtained using ad hoc real standards instead of the virtual pack standards supplied with the INCA software.

Fourier Transform-Infrared Spectroscopy (FT-IR). To identify the organic and inorganic components of the coating two FT-IR spectroscopy modes, transmittance-FT-IR (T-FT-IR) and diffuse reflectance infrared Fourier transform spectroscopy (DRIFTS) were used in order to discern the analytical mode that yields better results in terms of spectral resolution. Both FT-IR spectra were collected using a NICOLET spectrometer 20SXB. The instrument was connected to a Pentium 200, and the instrument software was OMNIC v 4.1, running under Windows 2000 Professional (Microsoft Corporation). The FT-IR spectra were registered from 3999 to 400 cm^{-1} with a resolution of 2 cm^{-1} and 200 scans. T-FT-IR spectra were obtained from KBr pellets prepared by uniformly mixing ~200 μg of powdered sample with KBr (1% wt). To better discriminate the Fresnel reflection, the SPECTRA-TECH attachment model COLLECTOR (Sutton, Surrey, England, SM1 1TH) was used to measure the diffuse reflectance in the FT-IR spectrometer. For DRIFT analyses, ~10 μg of powdered sample was mixed with KBr (3.5% wt) and the mixture was placed in a microsample cup (3 mm diameter).

Gas Chromatograph/Mass Spectroscopy (GC/MS). In addition to FT-IR spectroscopy, GC/MS was employed to identify the possible organic compounds present in the coating as described elsewhere.[31]

Methodological Approach to Characterize Black Ash and Bones. Conventional powder XRD and DRIFTS were performed to characterize material composition, since the coating characterization established the benefit of the latter vs T-FT-IR. Analytical instruments and protocols were applied similar to those specified for the brick and coating samples. For ^{14}C dating, bones were initially physically cleaned with ultrapurified water (MilliQ, Millipore) and then powdered to less than 1 mm in size. The bone powder was then digested in cold dilute acetic acid with constant agitation for 24 h to remove normal carbonates. Next, the bone powder was hydrolyzed under vacuum with HCl (37%) to dissolve bone apatite and evolve its carbon dioxide for analysis. To produce enough CO_2 for ^{14}C dating, the process was repeated three times requiring ~2000 g of bones. Then determination of the ^{14}C activity was realized using the Liquid Scintillation Counter PACKARD (Camberry Company) TRI-CARB 2560 TR/XL. The radiocarbon calibration program Calib Rev4.4.2 was used following the recommendations outlined by Stuiver and Reimer.[32] Determination is reported as conventional radiocarbon ages BP.

RESULTS AND DISCUSSION

Oven Bricks. Visual inspection of the bricks (Figure 2, left side) shows a color gradation from their original reddish-cream tone inside toward pistachio green and black at the external surface exposed to the oven temperature (refiring temperature). In situ melting evidence was observed including brick rounded contours, bubbles, and white salts. Conventional XRD of three samples taken from the color transitions was done to determine original minerals and newly formed phases occurring upon refiring. One advantage of this XRD method is its spatial resolution enabling suitable mineral detection and quantification. However, this method is not entirely apt to detect minerals present at very low amounts. XRD quantitative analysis showed that quartz was the main component (SiO_2, 28.1%, JCPDS 33-1161) followed by calcite ($CaCO_3$, 19.9%, JCPDS 05-0586), anorthite ($CaAl_2Si_2O_8$, 16.8%, JCPDS 20-0020), illite (mica-type clay mineral, general formula $(K,H_3O)(Al,Mg,Fe)_2(Si,Al)_4O_{10}[(OH)_2,(H_2O)]$, 14.3%, JCPDS 09-0343), diopside ($CaMgSi_2O_6$, 7.1%, JCPDS 19-0239), and hematite (Fe_2O_3, 4.3%, JCPDS 33-0664). The gypsum detected ($CaSO_4 \cdot 2H_2O$, 8.4%, JCPDS 33-0311) corresponds to salts formed at the brick surface, surely during burial.

Mineral evolution along the brick cross-section and penetration depth of temperatures in the brick upon refiring were better determine using μ-XRD. Figure 2 at the top right shows the 2D diffraction patterns of selected analyzed areas (no. 1, no. 3, no. 6) at the brick firing profile beginning from the surface (~1 mm, higher temperature, refiring temperature) inward (~20 mm, lower temperature, brick original temperature). A benefit of using 2D diffraction patterns is that they enable the differentiation of mineral phases, based on their different microstructural characteristics, more easily than conventional linear 2θ-scans. Continuous rings are produced by fine-grained mineral phases, while spotty rings are produced by coarse-grained mineral phases. Figure 2 at the bottom shows the sequence of the calculated 2θ scans corre-

(31) Romero-Noguera, J.; Bolívar-Galiano, F. C.; Ramos-López, J. M.; Fernández-Vivas, M. A.; Martín-Sánchez, I. *Inter. Biodeter. Biodegr.* **2008**, *62*, 427–433.

(32) Stuiver, M.; Remimer, P. J. *Radiocarbon* **1993**, *35*, 215–230.

sponding to the seven μ-XRD pinpoint analyses arranged from higher (no. 1) to lower temperature (no. 7). Minerals identified are indicated to better follow the firing transformations. Composition from the brick surface ~1 mm (diffractogram 1, Dif 1) to ~7 mm depth (Dif 3) reveals the presence of diopside (D), quartz (Q), and anorthite (A); this latter was absent at 7 mm depth (Dif 3) coinciding with the color change from black to green. At ~13 mm depth (Dif 5), the diopside diminishes, and at ~16 mm depth (Dif 6), it is no longer present, coinciding with the color change from green to cream; instead calcite (C) is detected in addition to quartz and illite (I). Finally in the brick interior, at ~20 mm depth (Dif 7) where the original brick texture and mineralogy is preserved, abundant quartz and calcite were identified, as well as lower amounts of illite.

It has been reported that in calcite-rich bricks, calcite starts to decompose at ~830−870 °C and that it reacts with silicates (i.e., quartz and clay minerals, e.g. illite) to form high temperature Ca-silicates (i.e., diopside, anothortite).[15] In carbonate-rich bricks such as ours, melting starts at lower temperature due to the fact that Ca and Mg from carbonates may act as melting agents.[33] The fact that calcite was detected at ~16 mm depth, but not at ~13 mm depth, indicates that the refiring temperature reached a depth of ~16 mm inside the brick. The presence of anorthite and diopside suggest that temperatures of 900−1000 °C were reached in the oven and that a Ca-rich raw material was used in the brick manufacture.[15] Anorthite starts to form at temperature >1000 °C in carbonate-rich bricks and diopside at ~900 °C at the dolomite−quartz interface.[15,34] In our bricks, anorthite was first detected at ~4 mm depth (Dif 2) and diopside until ~13 mm depth (Dif 5), which means that in the brick most external 5 mm, a temperature of ~1000 °C was attained, and from here to a ~13 mm depth the temperature was ~900 °C. The fact that diopside was detected implies that dolomite, $CaMg(CO_3)_2$ was used as raw material. Dolomite was not identified in the brick core because it decomposes at ~700 °C, a temperature far surpassed during brick manufacture. It should be mentioned that rapid heating may induce significant overstepping, thus formed phases can be often metastable.

The petrographical study of the brick revealed a gradual transition from the inside out in terms of mineralogy, matrix color, and pore morphology. Thus, elongated and connected pores in the original reddish-brown matrix modified to large, rounded, and isolated pores in a dark pistachio matrix at the surface. The brick interior preserved original clay minerals and calcite while the surface matrix was totally vitrified. Here, isolated grains of quartz were detected as temper, with angular morphology or embedded in micaschists (medium-grade metamorphic rocks rich in phyllosilicates). These latter crystals have lost their optical properties (birefringence and interference color) due to high firing temperature. We suggest that continuous use of the oven at ~900−1000 °C must have promoted brick partial melting as already observed by the naked eye.

SEM observations revealed extensive vitrification at the brick surface (Figure 3a). Round-shaped pores, due to melting of clay mineral particles and gas release,[35] develop the so-called "cellular texture".[34] Under higher magnification, the newly formed high-temperature phase (i.e., diopside according to XRD) was clearly discernible (Figure 3b). EDX analyses revealed that the matrix was Mg-free and rich in Si and Al with lower amounts of Ca and traces of Fe, while the new silicates, formed at the expenses of the matrix, contained significant amounts of Mg.

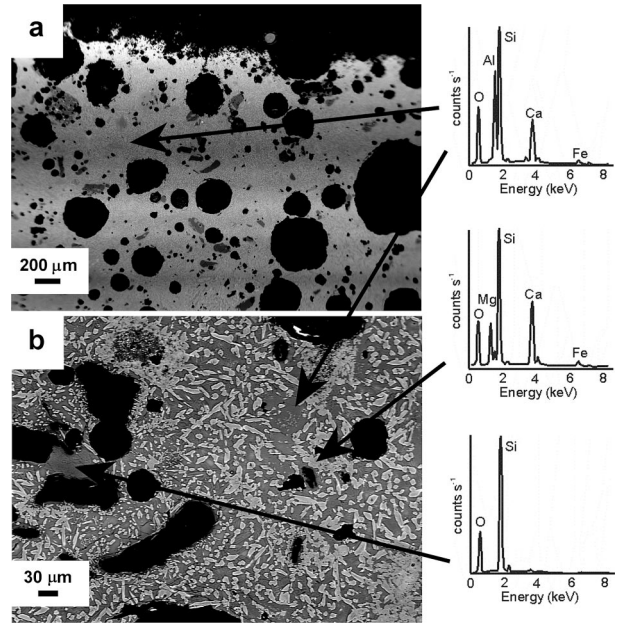

Figure 3. BSE images and EDX analyses of the brick sample: (a) general aspect of the brick surface showing rounded-shaped pores and (b) detail of prismatic diopside crystals dispersed in the matrix.

Wall Coating. *XRD Method.* The analysis with μ-DRX identified calcite and quartz but HAp was not detected. This may be due either to its absence or perhaps to the presence of very few crystals satisfying the Bragg diffraction condition. Rather, HAp was detected using the spin-mode XRD (<2%, JCPDS 09-0432) along with calcite and quartz.

Microscopic Techniques. Visual inspection revealed an orange-brown coating of ~1 mm thickness (Figure 1). The OM study showed that calcite constituted the aggregate and part of the binder where microfossils were also present. Other identified aggregates were quartz and micaschists. The observations suggest the use of geological materials from the immediate vicinity. These include the bioclastic calcarenite of Santa Pudia (Escuzar, Granada) and the micaschists proceeding from the Sierra Nevada.[36] Also acicular crystals of gypsum growing perpendicular to the wall fissures were observed. The clean contact between the coating and its support confirm its artificial origin.

Single point analysis using SEM-EDX revealed ubiquitous Ca in the coating (as binder and aggregate), attributed to calcite. Silicon was detected in the most abundant, largest, and irregularly shaped particles with a broad grain size distribution (~10−100 μm), suggesting the presence of quartz as an aggregate. Fewer amounts of smaller particles (<10−50 μm) also identified as aggregates were made of Mg and interpreted as dolomite. Scarce acicular crystals composed of Al, Si, Mg, and K were interpreted as illite. In the SE images, scarce angular grains of variable crystal

(33) Segnit, E. R.; Anderson, C. A. *Trans. Br. Ceram. Soc.* **1972**, *71*, 85–88.
(34) Tite, M. S.; Maniatis, Y. *Nature* **1975**, *257*, 122–123.
(35) Freestone, I. C.; Middleton, A. P. *Miner. Mag.* **1987**, *51*, 21–31.
(36) Puga, E.; Díazr de Federico, A.; Nieto, J. M.; Díaz Puga, M. A. *Est. Geol.* **2007**, *63*, 19–40.

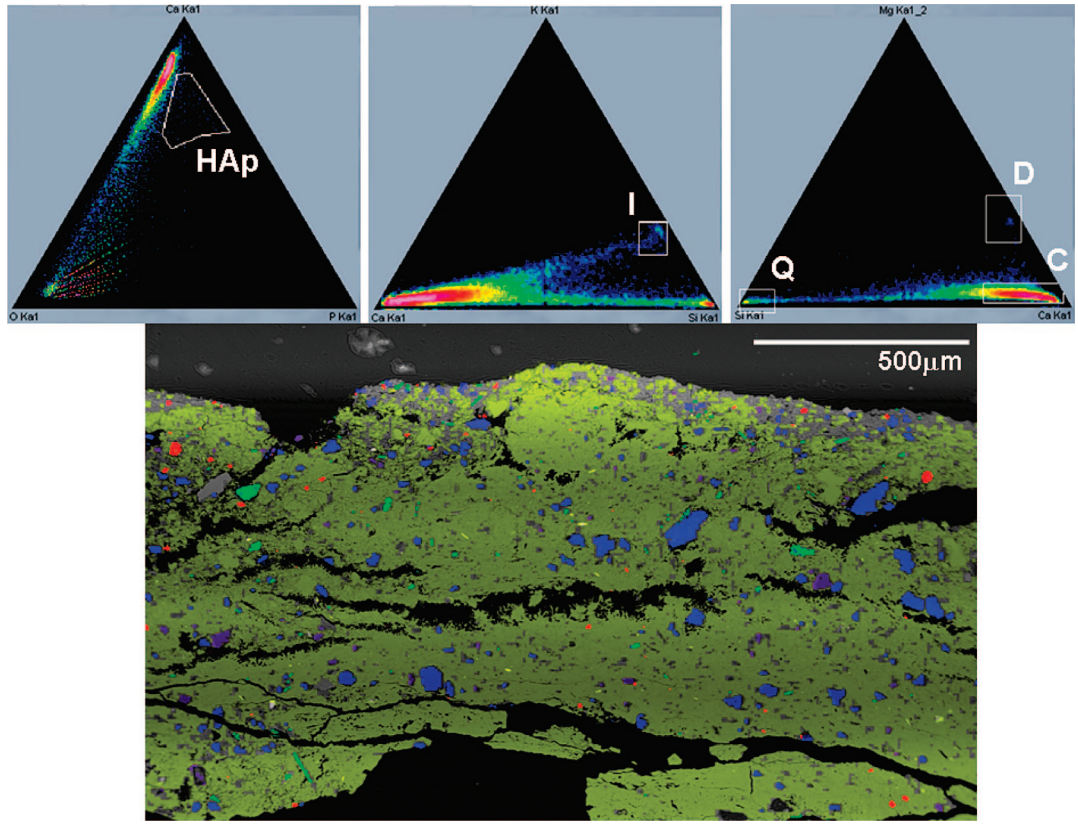

Figure 4. Ca−P−O, Ca−K−Si, and Mg−Ca−Si ternary phase diagrams (top). White boxes embedded the spots that correspond to the diverse mineral phases, namely, HAp = hydroxyapatite-like mineral; I = illite; Q = quartz; D = dolomite; C = calcite. False-color mineral map produced from SEM-EDX elemental mappings in the cross-section of the coating (bottom). Pistachio represents calcite, red represents HAp, blue represents quartz, purple represents dolomite, and green represents illite.

size below ~15 μm in diameter were seen. The pinpoint analyses identified Fe and Ti, attributed to hematite (Fe_2O_3) and rutile (Ti_2O), respectively. Phosphorus (P) was identified in the finest particles (<10 μm) dispersed in the coating. These particles, not easily observed with OM due to their small crystal size, were clearly identified in the compiled mineral map elaborated from SEM-EDX elemental maps. This mapping method particularly highlights the location and morphology of scarce and fine (micrometer size) crystalline components in cross-sectioned samples.

Since HAp was the relevant mineral sought in the coating, EDX spectral intensity ratios measuring relative concentrations of Ca, P, and O were extracted from the raw data for each pixel and plotted in a ternary composition diagram. Similarly, Ca−K−Si and Mg−Ca−Si ternary phase diagrams were plotted to visualize the distribution and morphology of quartz, calcite, dolomite, and illite. Figure 4 shows the ternary phase diagrams and the resulting mineral map. The false-color map shows that calcite was the most abundant (95.44%) and evenly distributed mineral in the coating. HAp was very scarce (0.33%) and randomly distributed as discrete, smoothed grains of sizes smaller than 40 μm. Other finely divided grains visualized in the map were uneven particles of angular quartz (3.48%), angular dolomite (0.48%), and needle-shaped illite (0.46%). Percents were balanced considering the contribution of the image black background. Although this imaging method efficiently identifies components and their distribution, it cannot establish their exact mineral composition.

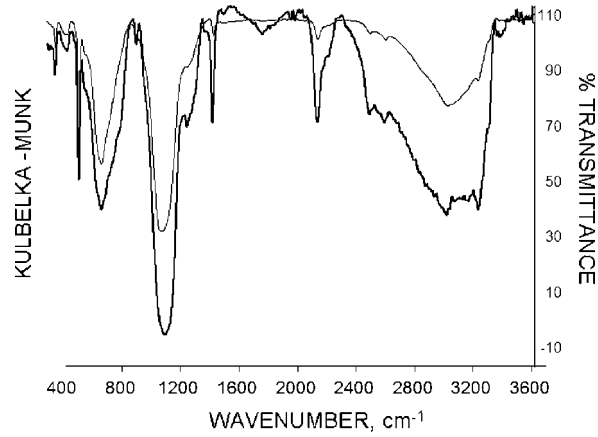

Figure 5. Wall coating DRIFT (solid line) and T-FT-IR (fine line) spectra.

T-FT-IR and DRIFT Spectroscopy. Figure 5 shows both T-FT-IR and DRIFT spectra of the coating sample. In both spectra, the position of the absorption bands are similar but relative intensities are clearly more intense in the case of DRIFT spectra.[37] Both spectra revealed the presence of HAp, as demonstrated by the P−O asymmetrical stretching band at 1100 cm^{-1} and the symmetrical stretching band at 912 cm^{-1}, as well as overlapped bands at ~660 cm^{-1} assigned to scissoring of O−P−O and

(37) Navas, N.; Romero-Pastor, J.; Manzano, E.; Cardell, C. *Anal. Chim. Acta* **2008**, *630*, 141–149.

bands at 3500 and 750 cm^{-1} showing O−H vibrations.[38] The remaining bands in the high wavenumber range (seen accurately only in the DRIFT spectrum) resulted from vibrations of O−H bonds. These bonds occur in water adsorbed in the hydroxyl groups present in the HAp structure. In addition, bands at 1450 cm^{-1} were ascribed to stretching vibrations of C═O which confirmed the existence of carbonate groups.[39] No collagen protein band was detected at ∼1650 cm^{-1}. Although carbonate groups are common in biological HAp,[39] in our study evidence suggests that they should proceed from contamination of the carbonate-base coating where the HAp grains are embedded. This theory is supported by visual observations showing that bones were thermally altered (change in color and trabecula modifications) and subsequently buried. Above 700 °C, carbonate groups start to decompose in bones, and at ∼800 °C, they disappear entirely, being replaced by lime (CaO).[39] Moreover the lack of collagen in our bones can be due either to exposure to temperatures higher than 650 °C or previous burial scenarios involving microbiological action.[40]

GC/MS Analysis. This technique did not detect in the coating any characteristic peaks that would indicate the occurrence of organic compounds, a fact which suggests that organic additives were not used as binders, supporting the FT-IR results (absence of amino acids from protein binders). Thus we can discard the possibility that the detected HAp was linked to the application of milk-derived, Ca caseinate-based protective treatments, or to the presence of egg white.[24]

Black Ash and Bone Strata. *XRD Methods.* Conventional XRD showed that the black ash was composed of calcite (40.7%, JCPDS 05-0586), muscovite (24.0%, JCPDS 07-0025), quartz (19.0%, JCPDS 33-1161), dolomite (10.3%, JCPDS 36-0426), and HAp (6.0% JCPDS 25-0166). The DRIFT spectrum was similar to that of the coating. The following absorption bands assigned to HAp were seen: the P−O asymmetrical stretching at ∼1100 cm^{-1} and the symmetrical stretching at ∼915 cm^{-1}, overlapped bands at ∼660 cm^{-1} assigned to O−P−O scissoring, and O−H vibration bands at 3500 and 750 cm^{-1}. Also bands at ∼1450 cm^{-1} confirmed the presence of carbonate groups, bands in the 1000−1100 cm^{-1} range proved the presence of silicate groups, and bands in the 3450−1625 cm^{-1} range confirmed the occurrence of adsorbed water. No collagen band was detected (1650 cm^{-1}).[38,39,41] Conventional XRD of the bones revealed that 95% was chlorian hydroxyapatite ($Ca_5(PO_4)_3$-(OH,Cl,F), JCPDS 25-0166) and 5% was calcite (JCPDS 05-0586). In biological HAp minerals, a large number and variety of substitutions can occur among similar ions, a process intensified due to burial, as is our case.[41] The DRIFT spectrum corroborated the presence of bands assigned to HAp, i.e., CO_3 vibration bands at 870, 1415, and 1460 cm^{-1} and PO_4 vibration bands at 565, 605, and 1035 cm^{-1}, as well as absence of any protein band. Bands associated with carbonate groups were not detected (1454−1460 cm^{-1}), which is consistent with the fact that these are burnt bones and that carbonates break down at temperature >700 °C.[15,34]

Radiocarbon Dating. Accurate ^{14}C dating of noncollagen bones is an unresolved challenge.[42] Collagen and its derivatives are the main components of bone targeted for ^{14}C dating. Thus dating poorly preserved bones such as ours (exposed to firing and burial scenarios) is difficult, and unreliable results may arise since the absence or scarcity of collagen increases the possible influence of contaminants which lead to uncertainty in the measured ^{14}C age.[41] Our ^{14}C measurement dated the age of the bones as 1600 ± 80 y A.D. This result should be interpreted with caution; the possibility of older ages for our bones cannot be excluded since, in addition to lacking collagen, they were subjected to postdepositional transformation and contaminations which could affect their "true" age.

CONCLUSIONS

The use of burnt bones as pigments (i.e., bone black and bone white, both animal charcoal produced at temperature of ∼800−900 °C, mostly formed by hydroxyapatite) was frequent in painting techniques throughout the history.[43] Their use in patinas of monuments is uncommon but has been reported in the literature in Greek, Roman, and Celtic buildings and medieval churches either with aesthetical intentions or to increase the patina mechanical strength.[7] Our results clearly identified hydroxyapatite (main component of bone pigments and animal bones) in the patina of the Nasrid wall. We discard the notion that the patina phosphorus content was linked to the accumulation of pigeon excrements since the walls are vertical. Instead the archeological evidence suggest that the bones found adjacent to the wall (well-defined stratigraphic section of ∼250 mm thick) were remains of the raw material used to manufacture powdered burnt-bone. This hypothesis is supported by the presence of a black ash layer below the bone layer and the scientific evidence that the temperature reached by the oven was high enough (∼1000 °C) to manufacture them. Despite this, considering the inaccurate ^{14}C dating of our bones due to problems when dating poorly preserved bones, we can not precisely identify when the coating was made. Nonetheless, it seems that the coating is coetaneous to the Moorish wall (1333−1354). However the results of this work are significant for archeologists since, to the authors' knowledge, this is the first report of both powder burnt bones in a patina on a Moorish monument, as well as the archeological artifacts (i.e., oven and raw materials) to produce them.

The innovative analytical methodologies applied in this work to typify the artifacts were very effective in giving insight into their composition and structure. This demonstrates the potential benefits of these approaches in characterizing artworks for conservation purposes and to resolve historical questions. The methods enable more rapid and precise analyses than traditional techniques. In particular the μ-XRD allows mineral identification of polycrystalline materials more efficiently than using standard powder XRD. Our μ-XRD method appears to be very effective for use in cultural heritage since it allows fast data acquisition (∼10 s) in a nondestructive way with moderately high spatial resolution

(38) López, M. E.; Echavarría, A.; Suárez, R.; Herrera, N. *Rev. Fac. Ing.* **2003**, *30*, 109–124.
(39) Haberko, K.; Bućko, M. M.; Brzeziśka-Miecznik, J.; Haberko, M.; Mozgawa, W.; Panz, T.; Pyda, A.; Zarębski, J. *J. Eur. Ceram. Soc.* **2006**, *26*, 537–542.
(40) Pijoan, C. M. A.; Mansilla, J.; Leboreiro, I. *Archaeometry* **2007**, *49*, 713–727.
(41) Petchey, F.; Higham, T. *J. Archaeol. Sci.* **2000**, *27*, 135–153.
(42) Surovell, T. A. *Geoarchaeology* **2000**, *15*, 591–608.
(43) Eastaugh, N.; Walsh, V.; Chaplin, T.; Siddall, R. *Pigment Compendium. A Dictionary of Historical Pigments*; Butterworth-Heineman: Oxford, U.K., 2004.

(~50−500 μm depending on the collimator used). Additionally it is an inexpensive technique that only requires applying adequate software to reduce 2D XRD data to 1D scans (i.e., XRD2Dscan software http://www.ugr.es/~anava/xrd2dscan.htm).

The visualization method of SEM-EDX-based mineral maps is also very promising for use in cultural heritage studies. It provided key information concerning the distribution of scarce mineral phases, size and grain shapes, and microtextural and structural characteristics that are overlooked when performing single-point analyses or elemental maps in artwork materials. However obtaining an excellent mineral map can be time-consuming since good elemental maps are required. Additionally until now DRIFTS spectra have barely been applied in heritage science but offer great potential for purposes of artwork identification thanks to the more intense vibrational bands (in contrast to the traditional T-FT-IR mode) and the need of lower sample amount.

ACKNOWLEDGMENT

This research was supported by the Andalusian Research Group RNM-179, Project HUM-2006-06210 and a research contract from Junta de Andalucia awarded to C. Cardell. We thank A. Kowalski for English revision and P. Alvarez-Lloret for helping with the bone study.

Received for review October 23, 2008. Accepted November 19, 2008.

AC8022444